ARCHIVES OF MECHANICS
Arch. Mech. **75** (5), 521–541, 2023, DOI: 10.24423/aom.4232

Shear properties of a honeycomb structure with zero Poisson's ratio

L. SONG[1)], Y. SUN[2)], Z. HAN[2)], T. WANG[1)], H. WANG[1)], C. YIN[1)], X. SHEN[1*)]

[1)] *State Key Laboratory of Mechanics and Control of Mechanical Structures, Nanjing University of Aeronautics and Astronautics, Nanjing, 210016, China*
[*)] *e-mail: shenx@nuaa.edu.cn (corresponding author)*

[2)] *Beijing Institute of Space Long March Vehicle, Beijing, 100076, China*

Honeycomb structures with zero Poisson's ratio show promising potential for application in variable-sweep wing aircraft. The shear properties of these honeycomb structures serve as a crucial indicator of their morphing capacity. This paper derives the linear and non-linear shear properties of a honeycomb structure with zero Poisson's ratio. A modified factor is introduced to establish a relationship between the linear and non-linear shear modulus of the honeycomb structure, simplifying the calculation method of the non-linear shear modulus. The validity of theoretical predictions is then confirmed using the finite element method. Furthermore, the influences of the geometric parameters on the shear properties of the honeycomb structure with zero Poisson's ratio are investigated, highlighting the varying contributions of these cell geometric parameters to the shear properties.

Key words: honeycomb structure, zero Poisson's ratio, shear properties, small deformation, large deformation.

1. Introduction

Honeycombs have higher porosity and lower mass density than their matrix materials due to the interconnected network of unit cells filling the internal space, thus resulting in high specific strength/stiffness and specific energy absorption [1–3]. The topology configuration of the repeating unit cells can significantly influence the mechanical properties of the honeycombs. Various topologies with different Poisson's ratio have been studied to date, including classical hexagonal [4] and triangular [5] honeycombs with positive Poisson's ratio (PPR), re-entrant [6], chiral [7, 8] and double V-shaped [8, 9] honeycombs with negative Poisson's ratio (NPR), as well as semi re-entrant [10] and semi-periodic sinusoidal [11] honeycombs with zero Poisson's ratio (ZPR). The structure with negative or positive Poisson's ratio expands or shrinks laterally when stretched in the axial direction. In contrast, a structure with ZPR will not deform lat-

erally under axial tension. Honeycombs with ZPR offer distinct advantages on some special occasions especially in the aviation field, when they can serve as a reliable support structure for flexible skin. These honeycombs provide sufficient out-of-plane stiffness to withstand surface aerodynamic loads while maintaining low in-plane stiffness to accommodate high strain capacity [12, 13]. In variable-sweep wing aircraft, honeycomb structures are subject to shear loads, making it crucial to accurately predict their equivalent shear properties for the convenient and efficient overall structure design [14].

The honeycomb structures are often assumed to be homogeneous and orthogonally anisotropic by predicting their equivalent properties in engineering [15, 16]. In recent years, extensive research has been conducted on the mechanical properties of honeycomb structures with ZPR, predominantly tensile and shear properties. Olympio *et al.* [17] proposed a hybrid honeycomb and an accordion cellular structure, providing elastic properties for these structures. Gong *et al.* [18] introduced a four-point star-shaped honeycomb structure with ZPR that can deform in two dimensions. Huang *et al.* [19] found that the cell-wall thickness and corner radius will affect the elastic characteristic of the two types of honeycombs with ZPR by means of the finite element method. Grima *et al.* [10] proposed a novel hexagonal honeycomb structure composed of both a conventional non-re-entrant form and an auxetic re-entrant form, and results show that they exhibit a zero Poisson's ratio in one direction and a higher than normal Young's modulus in the orthogonal direction. The equivalent elastic properties of the ZPR honeycomb structure with various elastic beams were deduced in detail by Liu *et al.* [11, 20, 21], Chen *et al.* [22] calculated the in-plane mechanics of an accordion honeycomb structure with ZPR under small deflection. To sum up, the review of the previous literature indicates that the effective elastic properties of honeycombs have been extensively studied under small deformation. However, the mechanical properties of honeycombs under large deformation considering geometric nonlinearity, are considerably more complicated than under small deformation. The Euler beam is employed to derive the effective elastic properties of the honeycombs. For the honeycombs with a large ratio of wall thickness to wall length, the influence of the shearing effect on the deformation of the honeycomb wall must be considered in deriving the effective elastic properties by the beam theory. Otherwise, it will cause significant errors [23, 24].

Considering geometric nonlinearity, the mechanical behavior of the honeycomb structures under large deflection differs significantly from that of small deflection, resulting in more complex mechanical properties. For non-linear mechanical performance research, Song *et al.* [25] deduced the nonlinear tensile and compressive modulus of the honeycomb structure with ZPR under large deflection without considering the shear deformation. Lan *et al.* [26] presented the non-linear constitutive relationship of traditional hexagonal honeycomb struc-

tures with PPR under shear load. FU *et al.* [14] studied the shear behavior of concave hexagonal honeycomb structures with NPR under large deflection. Soon afterward, ZHONG *et al.* [27] analyzed the nonlinear mechanical responses of the tetrachiral honeycomb structures with NPR under large deflection. However, there are limited reports on the theoretical study of the nonlinear shear properties of honeycomb structures with ZPR. To expand the application of honeycomb structures in the aviation field, it is necessary to consider the shear deformation of honeycomb structures with ZPR under both small and large deflection.

This paper aims to derive the shear properties of a honeycomb structure with ZPR under both small and large deflection. A modified factor is also introduced to characterize the relationship between linear and nonlinear shear modulus. Furthermore, the correctness of the linear and non-linear theoretical results was verified by the finite element simulation. Finally, a detailed analysis is conducted to examine the influence of the geometrical parameters of the honeycomb structure on its shear properties.

2. Theoretical analysis

Figure 1(a) shows a schematic diagram of the honeycomb structure with ZPR, where the x-direction and the y-direction represent the transverse and vertical directions, respectively. In the deformation analysis process, only the unit cell is considered as a homogeneous plate with effective modulus owing to the periodic substructure of the honeycomb structure [23], as illustrated in the red-marked area. Figure 1(b) illustrates the various parameters involved including h representing the length of the vertical walls, α representing the cell aspect ratio t denoting the thickness of all the walls, μ indicating the wall thickness ratio, l representing the length of inclined walls and θ (where $\theta = \pi - \varphi$) representing the internal angle between two walls.

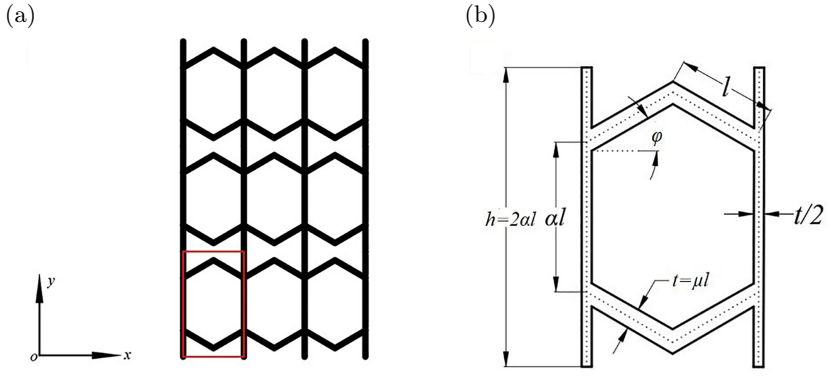

FIG. 1. Schematic diagram of the honeycomb structure with ZPR.

2.1. Linear shear properties

Figure 2 demonstrates the schematic diagram of the unit cell modeled to calculate the linear equivalent shear modulus of the ZPR honeycomb structure under small deformation where the fixed boundary is set at the left end of the model. The right end is set with a concentrated force F along the y-direction and a moment M along the x-direction.

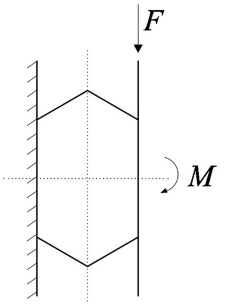

Fig. 2. Schematic illustration of unit cell model used to calculate the linear equivalent shear modulus.

According to the equilibrium equations, it can be concluded that the moment M is zero owing to the symmetry and:

$$F = \tau bh, \tag{2.1}$$

where b is the honeycomb's thickness perpendicular to the x-y plane.

The vertical deformation induced by a shear force can be obtained according to the Euler–Bernoulli beam theory [28]:

$$\delta = \frac{2\omega F l^3}{E_s I} \sin^2\theta, \tag{2.2}$$

where

$$\omega = \frac{4}{3} - \frac{12(\alpha + \cos\theta)^2}{\alpha^3 + 12\alpha^2 + 24\alpha\cos\theta + 16\cos^2\theta}. \tag{2.3}$$

According to the homogenization theory [29], it can be concluded that the shear strain is:

$$\gamma = \frac{\delta}{2l\sin\theta}. \tag{2.4}$$

According to the definition of the shear modulus, the homogenized and shear modulus can be written as:

$$G^*_{xy} = E_S \frac{\mu^3}{12\alpha\omega\sin\theta}, \tag{2.5}$$

where E_S is the equivalent shear modulus of the honeycomb structures with ZPR.

2.2. Nonlinear shear properties

The analysis in Section 2.1 is based on the small deformation assumption. This section analyzes the non-linear shear behavior of the honeycomb structure under large deflection. Figure 3 shows the schematic diagram of the theoretical model used to calculate the non-linear shear modulus of the honeycomb structure with ZPR. The homogeneous plate composed of four cell walls AB, CB, DB, and EB is selected as the representative analysis unit for analyzing the non-linear shear properties of the honeycomb structure with ZPR in this section, which is shown in the red rectangular dashed box in Fig. 3(a) [30]. It can be clearly observed from Fig. 3(b) that when the cell walls of the honeycomb structures are subjected to shear load, they will show anti-symmetric deformations about their respective midpoints [7].

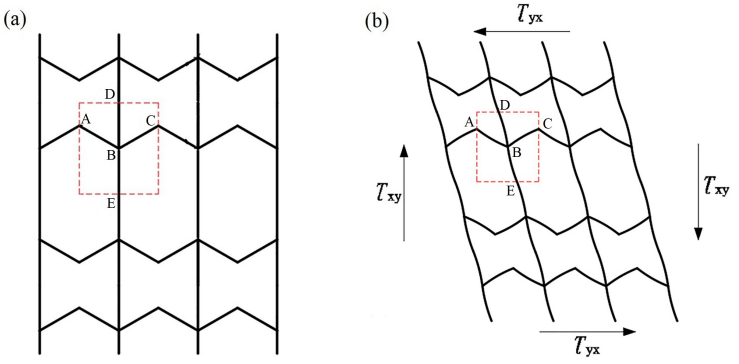

FIG. 3. Nonlinear analytical model of the honeycomb structure with ZPR.

Figure 4(a) shows the force distribution obtained from the analysis of the representative analysis unit under shear force applied to the honeycomb structure with ZPR. The deflection of the cell walls of the honeycomb structure is anti-symmetric, resulting in zero bending moments at sections A, B, C, and D. The forces received at these four sections are denoted as F_1, F_2, F_3, and F_4, respectively. Specifically, F_1 is parallel to F_2 and oriented y-direction, while F_3 is parallel to F_4 and oriented x-direction. Figure 4(b) illustrates the deflection results of the representative analysis unit.

As shown in Fig. 4(a), the shear stress, τ_{xy}, of the representative analysis unit is written as:

$$\tau_{xy} = F_3/(2bl\theta). \tag{2.6}$$

The shear strain, γ_{xy}, of the representative analysis unit can be written as:

$$\gamma_{xy} = \frac{u}{h} = \frac{x_{\mathrm{AB}} + x_{\mathrm{CB}} + x_{\mathrm{DB}} + x_{\mathrm{EB}} - 2l\sin\theta}{h} \tag{2.7}$$

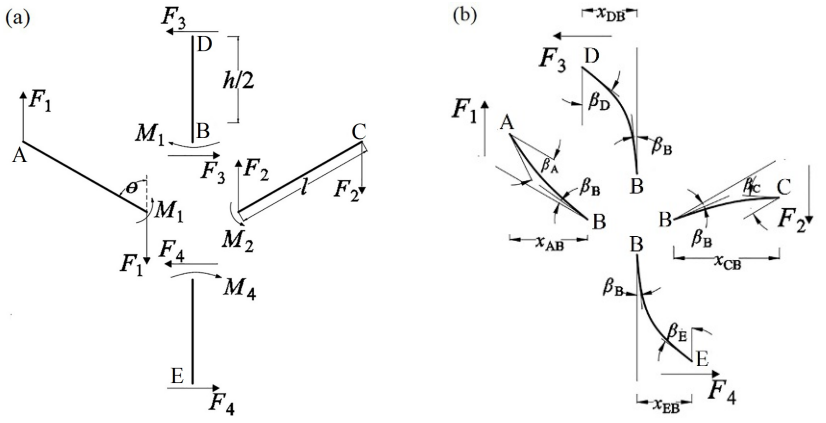

FIG. 4. Representative analysis unit of the honeycomb structure with ZPR under shear load.

with

$$u = x_{AB} + x_{CB} + x_{DB} + x_{EB} - 2l\sin\theta, \tag{2.8}$$

where u is the sum of the displacements of the four points A, C, D, and E along the x-direction; x_{AB}, x_{CB}, x_{DB}, and x_{EB}, respectively, correspond to the projection lengths of the deformed walls AB, CB, DB, and EB on the x-axis. Finally, the shear modulus of the honeycomb structure with ZPR is solved by combining Eqs. (2.6) and (2.7):

$$G_{xy} = \frac{\tau_{xy}}{\gamma_{xy}} = \frac{F_3}{u} \cdot \frac{\alpha}{2b\sin\theta}. \tag{2.9}$$

In order to represent the curve length of each deformed cell wall, we establish a curve coordinate system denoted by s, with points A, C, D, and E serving as the starting points. Let us consider the deflection of the wall AB as an example. The deflection of the inclined wall AB under the action of the applied force is depicted in Fig. 5. Here, s represents the length of the deformed curved wall AB starting from point A, while β denotes the angle between the tangent of a point on the deformed curve AB and the original wall AB. The angle β at sections A and B is denoted as β_A and β_B, respectively. Based on the elastic bending theory of beam [28], the second order differential equation for the wall AB is obtained from:

$$E_S I \frac{d^2\beta}{ds^2} = -F_1 \sin(\theta - \beta), \tag{2.10}$$

where I represents the second moment of inertia of the cell wall which states that $I = bt^3/12$. Then, Eq. (2.10) can be further transformed into

$$\frac{d\beta}{dS} = -2\pi\overline{f_1}\sqrt{\cos^2(\theta/2 - \beta_A/2) - \cos^2(\theta/2 - \beta/2)}, \tag{2.11}$$

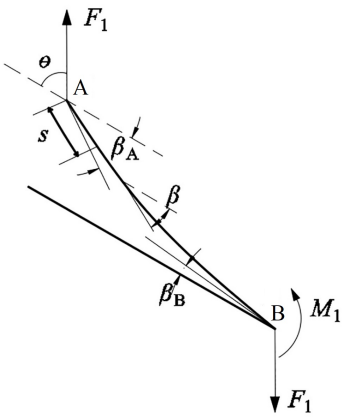

FIG. 5. Deflection of the inclined cell wall AB.

where $S = s/l$ denotes the length of the dimensionless curved wall AB, and

$$\overline{f}_1 = \sqrt{\frac{F_1}{P_{cr1}}} = \sqrt{\frac{F_1}{\pi^2 E_S I/l^2}} \tag{2.12}$$

is the introduced dimensionless force $P_{cr1} = \frac{\pi^2 E_S I}{l^2}$.

Equation (2.11) can be further rewritten as the following expression:

$$dS = -\frac{d\beta}{2\pi\overline{f_1}\cos(\theta/2 - \beta_A/2)\cos\eta} = -\frac{d\eta}{\pi\overline{f_1}\sin(\theta/2 - \beta/2)} \tag{2.13}$$

with

$$\eta = \arcsin\left(\frac{\cos(\theta/2 - \beta/2)}{\cos(\theta/2 - \beta_A/2)}\right). \tag{2.14}$$

Then, use the elliptic integral to adapt the dimensionless force $\overline{f_1}$ as:

$$\overline{f}_1 = \frac{2}{\pi}[F(m) - F(\eta_1, m)] = \frac{2}{\pi}\int_{\eta_1}^{\pi/2} \frac{1}{\sqrt{1 - m^2\sin^2\eta}} d\eta, \tag{2.15}$$

where

$$m = \cos(\theta/2 - \beta_A/2), \tag{2.16}$$

$$\eta_1 = \arcsin\left(\frac{\cos(\theta/2 + \beta_B/2)}{\cos(\theta/2 - \beta_A/2)}\right), \tag{2.17}$$

$$F(m) = \int_0^{\pi/2} \frac{1}{\sqrt{1 - m^2 \sin^2 \eta}}\, d\eta, \tag{2.18}$$

$$F(\eta_1, m) = \int_0^{\eta_1} \frac{1}{\sqrt{1 - m^2 \sin^2 \eta}}\, d\eta. \tag{2.19}$$

Combining Eqs. (2.13)–(2.15), it can be derived that the bending moment of the cell wall AB at section B is:

$$\begin{aligned} M_1 &= E_S I \left.\frac{d\beta}{dS}\right|_{S=1} \\ &= 4\sqrt{2} E_S I [F(m) - F(\eta_1, m)] \sqrt{\cos(\theta - \beta_{\mathrm{A}}) - \cos(\theta + \beta_{\mathrm{B}})}. \end{aligned} \tag{2.20}$$

Based on the geometric relationship in Fig. 5, the projection length expression of the deformed curved wall AB on the x-axis can be derived as:

$$x_{\mathrm{AB}} = l \int_0^1 \cos[\pi/2 + (\theta - \beta)]\, dS = l \frac{2\cos(\theta/2 - \beta_{\mathrm{A}}/2)\cos\eta_1}{F(m) - F(\eta_1, m)}. \tag{2.21}$$

Similar to the way to derive x_{AB} and $\overline{f_1}$ related to wall AB, the force exerted on the cell wall CB and its projection length on the x-axis can be obtained. The solved expression of the dimensionless force $\overline{f_2}$ is as follows:

$$\overline{f_2} = \sqrt{\frac{F_2}{P_{cr2}}} = \frac{2}{\pi}[F(m) - F(\eta_2, m)], \tag{2.22}$$

where

$$P_{cr2} = \frac{\pi^2 E_S I}{l^2}, \tag{2.23}$$

$$F(m) = \int_0^{\pi/2} \frac{1}{\sqrt{1 - m^2 \sin^2 \eta}}\, d\eta, \tag{2.24}$$

$$F(\eta_2, m) = \int_0^{\eta_2} \frac{1}{\sqrt{1 - m^2 \sin^2 \eta}}\, d\eta, \tag{2.25}$$

with

$$m = \cos((\pi - \theta)/2 - \beta c/2), \tag{2.26}$$

and

$$\eta_2 = \arcsin\left(\frac{\cos((\pi-\theta)/2+\beta_{\mathrm{B}}/2)}{\cos((\pi-\theta)/2-\beta_{\mathrm{C}}/2)}\right). \tag{2.27}$$

The bending moment of the wall CB at section B can be written as:

$$M_2 = 4\sqrt{2}E_S[F(m)-F(\eta_2,m)] \times \sqrt{\cos((\pi-\theta)-\beta_{\mathrm{C}})-\cos((\pi-\theta)+\beta_{\mathrm{B}})}. \tag{2.28}$$

The projection length expression of the deformed curved wall AB on the x-axis can be derived as:

$$x_{\mathrm{CB}} = l\int_0^1 \cos[\pi/2+((\pi-\theta)-\beta)]\,dS = l\frac{2\cos((\pi-\theta)/2-\beta c/2)\cos\eta_2}{F(m)-F(\eta_2,m)}, \tag{2.29}$$

where

$$E(m) = \int_0^{\pi/2}\sqrt{1-m^2\sin^2\eta}\,d\eta, \tag{2.30}$$

$$E(\eta_2,m) = \int_0^{\eta_2}\sqrt{1-m^2\sin^2\eta}\,d\eta. \tag{2.31}$$

The deflection of the vertical wall DB under the action of force F_3 is shown in Fig. 3(a). The second order differential equation for the wall DB is obtained from the following:

$$E_S I\frac{d^2\beta}{ds^2} = -F_3\sin\left(\frac{\pi}{2}-\beta\right). \tag{2.32}$$

Adopting a calculation process similar to the derivation of the mechanical parameters of the inclined wall, the solved expression of the dimensionless force $\overline{f_3}$ is as follows:

$$\overline{f_3} = \sqrt{\frac{F_3}{P_{cr3}}} = \frac{2}{\pi}[F(m)-F(\eta_3,m)], \tag{2.33}$$

where

$$P_{cr3} = \frac{\pi^2 E_S I}{h^2}, \tag{2.34}$$

$$F(m) = \int_0^{\pi/2}\frac{1}{\sqrt{1-m^2\sin^2\eta}}\,d\eta, \tag{2.35}$$

$$F(\eta_3, m) = \int_0^{\eta_3} \frac{1}{\sqrt{1 - m^2 \sin^2 \eta}}\, d\eta, \tag{2.36}$$

where

$$m = \cos(\pi/4 - \beta_{\mathrm{D}}/2) \tag{2.37}$$

and

$$\eta_3 = \arcsin\left(\frac{\cos(\pi/4 + \beta_{\mathrm{B}}/2)}{\cos(\pi/4 - \beta_{\mathrm{D}}/2)}\right). \tag{2.38}$$

Combining Eqs. (2.32) and (2.33) the bending moment of the wall DB at section B can be written as:

$$\begin{aligned} M_3 &= E_S I \frac{d\beta}{dS}\bigg|_{S=0.5} \\ &= 2\sqrt{2} E_S I [F(m) - F(\eta_3, m)] \sqrt{\cos(\pi/2 - \beta_{\mathrm{D}}) - \cos(\pi/2 + \beta_{\mathrm{B}})}. \end{aligned} \tag{2.39}$$

The projection length expression of the deformed curved wall DB on the x-axis can be derived as:

$$x_{\mathrm{DB}} = h \int_0^1 \cos(\pi/2 - \beta)\, dS = \frac{h}{2} - \frac{[E(m) - E(\eta_3, m)]}{F(m) - F(\eta_3, m)} h, \tag{2.40}$$

where

$$E(m) = \int_0^{\pi/2} \sqrt{1 - m^2 \sin^2 \eta}\, d\eta, \tag{2.41}$$

$$E(\eta_3, m) = \int_0^{\eta_3} \sqrt{1 - m^2 \sin^2 \eta}\, d\eta. \tag{2.42}$$

The deflection of the wall EB and the wall DB are the same, and the dimensionless parameter, $\overline{f_4}$, the moment, M_4, and the projection length of deformed curved wall EB on the x-axis, x_{EB}, are obtained in the same way.

As shown in Fig. 3, the resultant force received by the representative analysis unit in the x-direction and y-direction are respectively equal to zero, that is, $\sum F_x = 0$ and $\sum F_y = 0$, we can further obtain:

$$\overline{f}_1 = \overline{f_2}, \tag{2.43}$$

$$\overline{f}_3 = \overline{f_4}. \tag{2.44}$$

The bending moments at node B have the relationship of $M_1+M_2 = M_3+M_4$, and Eq. (2.45) can be obtained by substituting Eqs. (2.20), (2.28), and (2.39) into it, as follows:

$$
\begin{aligned}
(2.45)\qquad & 2\overline{f_1}\sqrt{\cos(\theta-\beta_{\mathrm{A}})-\cos(\theta+\beta_{\mathrm{B}})} \\
& \quad + 2\overline{f_2}\sqrt{\cos((\pi-\theta)-\beta_{\mathrm{C}})-\cos((\pi-\theta)+\beta_{\mathrm{B}})} \\
& = \overline{f_3}\sqrt{\cos(\pi/2-\beta_{\mathrm{D}})-\cos(\pi/2+\beta_{\mathrm{B}})} \\
& \quad + \overline{f_4}\sqrt{\cos(\pi/2-\beta_{\mathrm{E}})-\cos(\pi/2+\beta_{\mathrm{B}})}.
\end{aligned}
$$

In addition, according to the shear stress reciprocity theorem, the force equilibrium formula in Fig. 4(a) is given by:

$$
(2.46)\qquad \frac{F_1}{2h} = \tau_{xy} = \tau_{yx} = \frac{F_3}{2l\sin\theta}.
$$

This paper uses Matlab to calculate the equations composed of Eqs. (2.33), (2.43), and (2.46) numerically. A specific value is assigned to F_3 in the equation to derive the values of β_A, β_B, β_C, β_D, and β_E. Those obtained values are then substituted into Eqs. (2.8), (2.21), (2.29), and (2.40) to solve for the combined displacements u at points A, C, D, and E. Finally, substituting u into Eq. (2.9) to solve the shear modulus of the honeycomb structure with ZPR.

The relationship between the linear and non-linear shear modulus of the honeycomb structure with ZPR is expressed as follows:

$$
(2.47)\qquad G_{xy} = kG^*_{xy},
$$

where k is the non-linear modified factor to establish the relationship between the shear modulus of the honeycomb structure under small and large deflection.

By solving Eqs. (2.5), (2.9), (2.21), (2.29), (2.40), and (2.47), the expression of the non-linear modified factor k can be obtained as:

$$
(2.48)\qquad k = \frac{\overline{f_3}^2\pi^2 lw}{2}\,\frac{1}{x_{\mathrm{AB}}+x_{\mathrm{CB}}+x_{\mathrm{DB}}+x_{\mathrm{EB}}-2l\sin\theta}.
$$

It can be seen from Eq. (2.48) that the non-linear modified factor k is related to the geometric structure of the honeycomb structure but not independent of the wall thickness ratio μ, so the change in the relative density will not affect the non-linear modified factor k.

3. Finite element simulation

This section employed the commercial finite element (FE) software ABAQUS (version 6.14) to conduct numerical simulation and validate the linear and non-linear shear theoretical results obtained by the above-mentioned methods. The

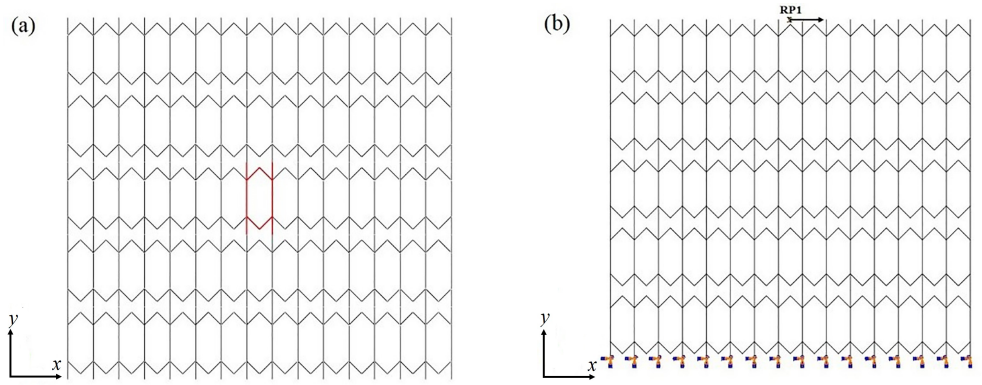

FIG. 6. (a) FE model and (b) boundary conditions of the honeycomb structure with ZPR.

material properties considered were an aluminum alloy with an elastic modulus of 76 GPa and Poisson's ratio of 0.33. The full-size representative volumes were given by 5*17 unit cells, as shown in Fig. 6(a). The elements used in the models have constant linear elastic and isotropic material properties. A 2-node linear element B21 is used to model the honeycomb block with an element size of 0.1 mm. The lower boundary is set as a fixed support constraint, and the points on the upper boundary are coupled to apply displacement along the x-direction to ensure that the upper and lower boundaries are parallel to each other after deflection, as shown in Fig. 6(b). In order to avoid Saint-Venant effects from the borders, the stress and strain were calculated within the central unit cell (red section in Fig. 6(a)) [31]. For linear FE simulation, refer to Fig. 1(b) to model the geometric structure in the simulation and consider the influence of geometric configuration on the linear shear modulus from three aspects: the cell aspect ratio α, the wall thickness ratio μ, and the internal angle θ. An internal geometric parameter of $l = 10$ mm was adopted. The simulation was carried out with $\alpha = 2$, $\mu = 0.15$, $b = 1$ mm and θ ranged from 20° to 45° with even step at 5°. For the non-linear FE simulation, the geometric parameters of the unit cell are $l = 10$ mm, $\theta = 45°$, $b = 1$ mm, $\alpha = 2$, $\mu = 0.15$. The shear strain, γ_{xy}, is defined as the displacement of the upper boundary of the central unit cell in the x-direction divided by its original projection in the y-direction. Similarly, the shear stress, τ_{xy}, is calculated as the force acting on the upper boundary of the central unit cell divided by its original projection in the x-direction. The relative percentage error is given as follows:

$$Error(\%) = \frac{|\omega_{theoretical} - \omega_{FEM}|}{\omega_{theoretical}} \times 100\%,$$

where $\omega_{theoretical}$ and ω_{FEM} are the theoretical and simulation results, respectively.

Figure 7 shows the theoretical and FE results of linear effective shear properties of the ZPR honeycomb structure under different internal angles. One can see that the theoretical predictions of the shear modulus are consistent with the simulation results. The mean relative percentage error for the shear modulus is 1.2% with a maximum deviation of 1.5% and a minimum of 0.9%. It should be noted that the simulation results are somewhat below the theoretical ones, contributing to the difference between the simulation model and the theoretical model [32]. The FE results of the honeycomb structure with 17*5 unit cells are also depicted in Fig. 7. It can be found that there are minimal differences in the FE results between 5*17 and 17*5 unit cells. If the forces acting on a small portion of the surface of an elastic body are replaced by another statically equivalent system of forces acting on the same portion of the surface, this redistribution of loading produces substantial changes in the stresses locally but has a negligible effect on the stresses at distances which are large in comparison with the linear dimensions of the surface on which the forces are changed [33].

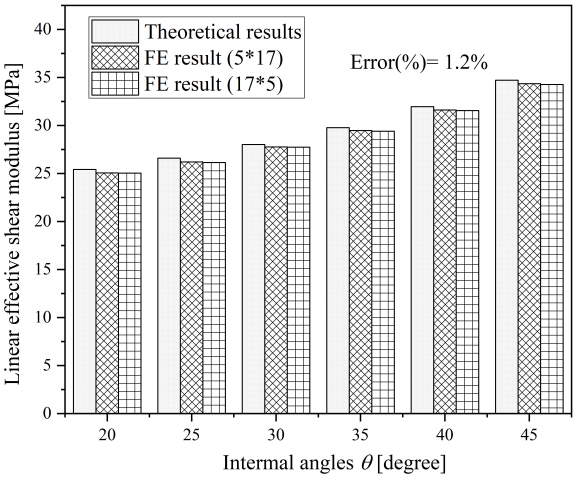

FIG. 7. Theoretical and simulation results of linear effective shear properties of the ZPR honeycomb structure.

Figure 8 presents a comparison of the stress-strain curve of non-linear theoretical results linear theoretical results and the FE results (5*17) with dimensionless shear stress. The non-linear theoretical results exhibit slightly higher values compared to the FE results. The three curves coincide well when γ_{xy} is less than 0.15. However, as the strain increases, the FE results and non-linear theoretical results gradually deviate from linear theoretical results, with the non-linear theoretical results matching the FE results. These discrepancies between the analytical and FE results can be attributed to several reasons. Firstly the FE simulation utilizes the Timoshenko beam model, while the theoretical analysis employs the

Euler–Bernoulli beam model, resulting in the FE results being slightly lower than the analytical ones [18]. Secondly, the deformation of the vertical wall of the honeycombs is disregarded. Figure 8 validates the accuracy of the analytical formulas derived in Section 2.2.

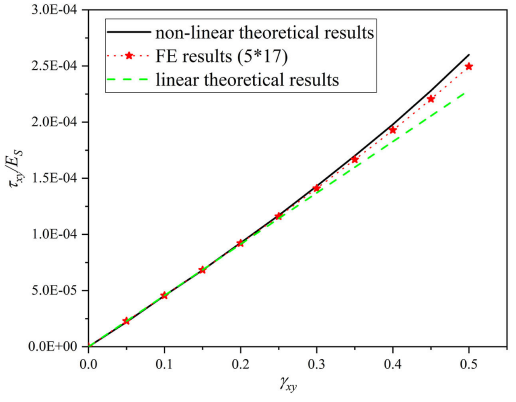

Fig. 8. Stress-strain relationship of the honeycomb structure with ZPR.

4. Results and discussions

In this section, theoretical calculations are carried out to explore the influences of the geometric parameters on the shear properties of the honeycomb structure with ZPR.

Figure 9 illustrates the effects of α and μ on the linear shear modulus G^*_{xy} of the honeycomb structure with ZPR versus θ. When α and μ are held constant,

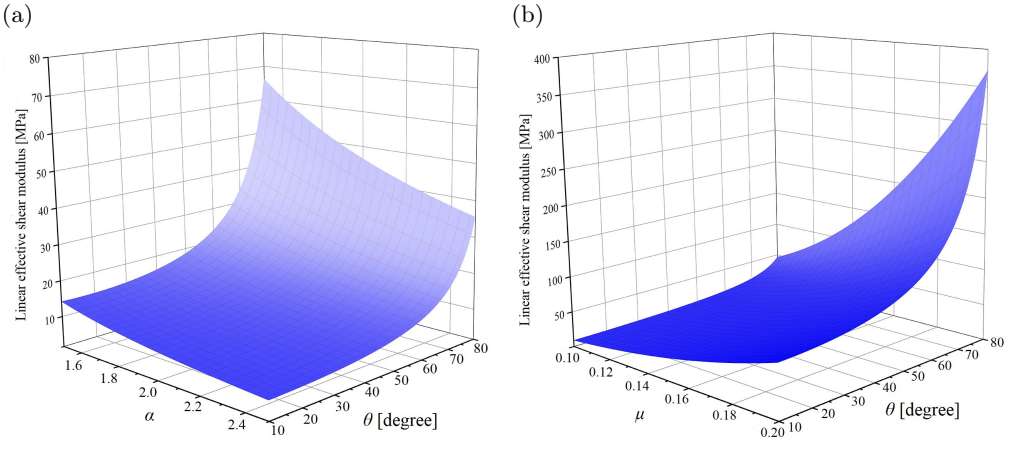

Fig. 9. The effects of (a) α and (b) μ on the linear shear modulus G^*_{xy} of the honeycomb structure with ZPR versus θ.

G^*_{xy} gradually decreases with increasing θ. As shown in Fig. 9(a), keeping θ and α constant, G^*_{xy} increases as μ increases. Furthermore Fig. 7(b) reveals that when θ and μ remain constant, an increase in α results in a decrease in G^*_{xy}.

According to Eq. (2.9) $\gamma_{xy}\alpha$ and θ administrate G_{xy}/E_S of the honeycomb structure with ZPR. Figures 10 and 11 plot the relationship between the geometric configuration and the dimensionless nonlinear shear modulus G_{xy}/E_S. It can be distinctly found that G_{xy}/E_S increases with γ_{xy} but decreases with an increase in α and θ.

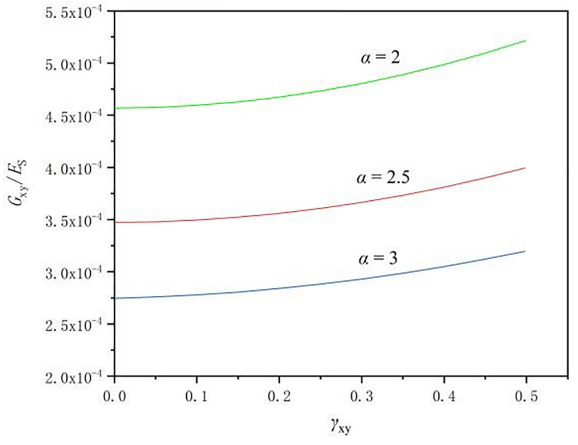

FIG. 10. The influences of cell aspect ratio α and shear strain, γ_{xy} on the dimensionless nonlinear shear modulus with $\mu = 0.15$, $\theta = 45°$.

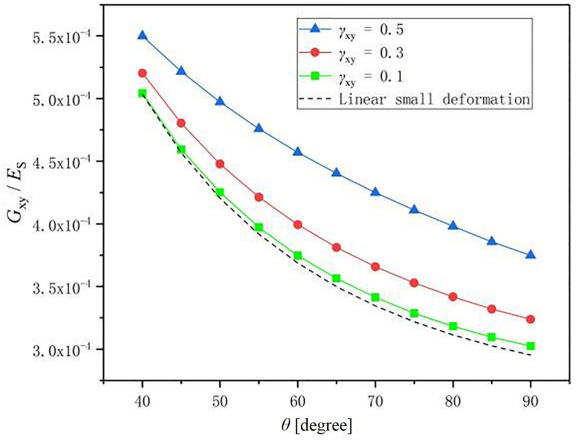

FIG. 11. The influences of internal angle θ on the dimensionless nonlinear shear modulus with $\mu = 0.15$, $\alpha = 2$.

The relative density ρ_r is generally considered to be a crucial parameter that determines the shear properties of honeycomb structures. The relative density expression of the honeycomb structure is:

$$\rho_r = \frac{\rho^*}{\rho_s} = \frac{ht + 2lt}{2hl\sin\theta}, \tag{4.1}$$

where ρ^* and ρ_s represent the density of the honeycomb structure and the raw material, respectively. Equation (2.49) gives the mathematical relationship between relative density ρ_r and geometric parameters of the honeycomb structure. By fixing θ and α, the relative density ρ_r can be maintained constant by altering the thickness t. Utilizing numerical calculations in Matlab

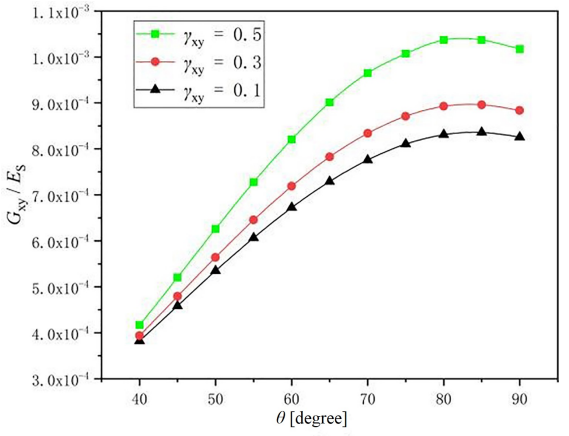

FIG. 12. The influences of internal angle θ with $\alpha = 2$ and $\rho_r = 0.212$.

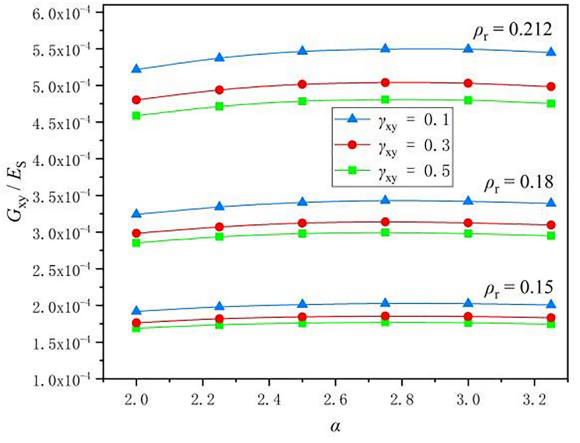

FIG. 13. The influences of cell aspect ratio α with $\theta = 45^\circ$ and $\rho_r = 0.212$, 0.18, 0.15.

we can determine the effects of θ and α on G_{xy} of the honeycomb structure with ZPR. Figure 12 illustrates that for a fixed l of 10 mm, α of 2 and ρ_r of 0.212, G_{xy} increases with increasing θ, reaching a maximum at approximately 85° and then decreases. Additionally, considering $l = 10$ mm, $\theta = 45°$ and varying relative density of $\rho_r = 0.212$, 0.18, and 0.15, it can be found from Fig. 13 that G_{xy} increases with α, reaching a maximum at around 2.75 and then decreases. Furthermore Fig. 13 demonstrates that G_{xy} increases with the increasing relative density.

The modified factor k establishes the relationship between the shear modulus of the honeycomb structure under small deflection and large deflection Eq. (2.48) reveals that α and θ play a significant role in determining the value of k. Nu-

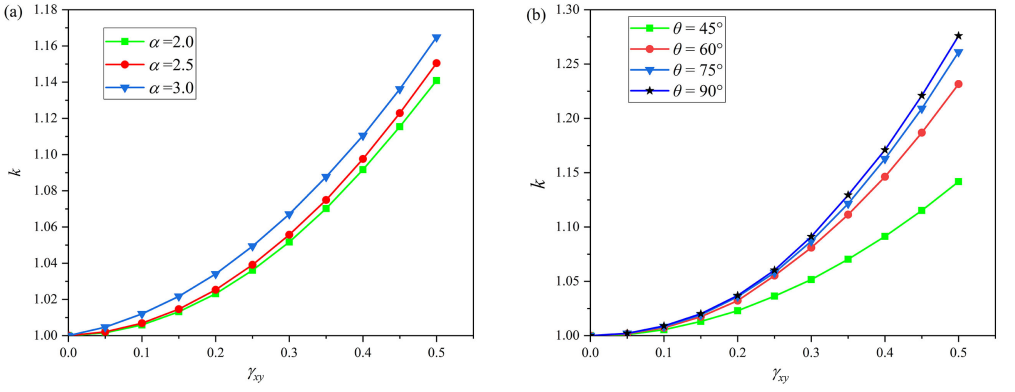

FIG. 14. The influences of cell aspect ratio α and internal angle θ on the modified factor k.

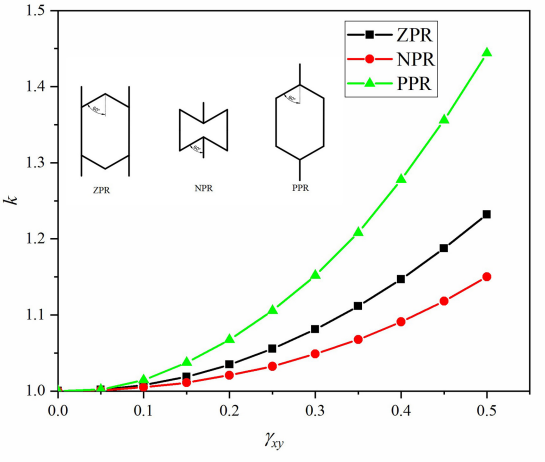

FIG. 15. Comparison of the modified factor k of ZPR, NPR and PPR honeycomb.

merical calculations demonstrates that the value of k starts at 1 and increases with γ_{xy}, as well as with an increase in α and θ, as depicted in Fig. 14. This parameter, k, not only explains the disparity between the linear and non-linear shear modulus but also enables the quick determination of the non-linear shear modulus when the linear shear modulus is known.

Conventional, re-entrant hexagonal honeycombs with NPR and regular hexagonal honeycombs with PPR are widely used in engineering. Thus, to distinguish the differences in shear mechanical properties among the honeycomb with ZPR, NPR and PPR, three honeycombs with $\theta = 60°$ are selected to compare their modified factor k. The variation in k value for PPR and NPR honeycombs was consistent with that of ZPR honeycombs. That is to say, the k value of the three honeycombs starts from 1 and increases with the increase of shear strain, γ_{xy}. In addition, k value of regular hexagonal honeycombs with PPR is larger than that of honeycomb with ZPR and NPR while the k value of honeycombs with NPR is the smallest. The variations of the k value of the honeycomb with ZPR, NPR and PPR are related to their effective area.

5. Conclusions

In this work, the linear and non-linear effective shear modulus of the honeycomb structure with ZPR under small deflection and large deflection has been derived by the Euler–Bernoulli beam theory and the elastic bending beam theory. The FE results validate the correctness and effectiveness of the theoretical predictions. Results reveal that the linear shear modulus increases with the wall thickness ratio μ but decreases with the cell aspect ratio α and the internal angle θ. On the other hand, the nonlinear shear modulus increases with shear strain but decreases with α and θ. For $\alpha = 2$ and $\rho_r = 0.212$, the nonlinear shear modulus of the honeycomb structure with ZPR increases with increasing θ, reaching the maximum at approximately 85° and then decreases. Similarly, when θ and ρ_r are kept constant, the nonlinear shear modulus increases as α increases reaching a maximum at around 2.75 and then decreases. The modified factor, k, exhibits an increasing trend with shear strain and increases with α and θ, indicating a more pronounced difference between the linear and non-linear shear modulus; k allows for converting the linear shear modulus under small deflection to the non-linear shear modulus under large deflection. Importantly, k is independent of relative density, simplifying the calculation of the non-linear shear modulus for honeycomb structures with varying relative densities.

Overall, this study serves as a valuable manual for designing ZPR honeycomb structures, facilitating the configuration design to meet the shear performance requirements in different engineering applications and under various conditions.

Acknowledgements

This work was supported by the National Natural Science Foundation of China under Grant No. 11872207, Aeronautical Science Foundation of China under Grant No. 20180952007, Foundation of National Key Laboratory on Ship Vibration and Noise under Grant No. 614220400307, research project funded by Ministry of Industry and Information under Grant No. 1001-DAB22015 and the National Key Research and Development Program of China under Grant No. 2019YFA708904.

References

1. R. YU, W. LUO, H. YUAN, J. LIU, W. HE, Z. YU, *Experimental and numerical research on foam filled re-entrant cellular structure with negative Poisson's ratio*, Thin-Walled Structures, **153**, 106679, 2022.
2. Y. ZHU, Q. QIN, J. ZHANG, *On effective mechanical properties of an orthogonal corrugated sandwich structure*, Materials & Design, **201**, 109491, 2021.
3. V.H. NAM, V.M. DUC, C.V. DOAN, N.T.T. XUAN, N.T. PHUONG, *Nonlinear postbucking behavior of auxetic-core toroidal shell segments with Graphene reinforced face sheets under axial loads*, Archives of Mechanics, **74**, 89–108, 2022.
4. T.C. HALES, *The honeycomb conjecture*, Discrete & Computational Geometry, **25**, 1–22, 2001.
5. A.J. WANG, D.L. MCDOWELL, *In-plane stiffness and yield strength of periodic metal honeycomb*, Journal of Engineering Materials and Technology, **126**, 137–156, 2004.
6. L.L. HU, M.Z. ZHOU, H. DENG, *Dynamic crushing response of auxetic honeycombs under large deformation: Theoretical analysis and numerical simulation*, Thin-Walled Structures, **131**, 373–384, 2018.
7. C. QI, F. JIANG, C. YU, S. YANG, *In-plane crushing response of tetra-chiral honeycombs*, International Journal of Impact Engineering, **130**, 247–265, 2019.
8. Q.T. DENG, Z.C. YANG, *Effect of Poisson's ratio on functionally graded cellular structures*, Materials Express, **6**, 461–472, 2016.
9. X. ZHAO, Q. GAO, L. WANG, Q. YU, Z.D. MA, *Dynamic crushing of double-arrowed auxetic structure under impact loading*, Materials & Design, **160**, 527–537, 2018.
10. J.N. GRIMA, L. OLIVERI. D. ATTARD, B. ELLUL, R. GATT, G. CICALA, G. RECCA, *Hexagonal honeycomb with zero Poisson's ratio and enhanced stiffness*, Advanced Engineering Materials, **12**, 855–862, 2010.
11. W.D. LIU, H.J. LI, J. ZHANG, Y.L. BAI, *In-plane mechanics of a novel cellular structure for multiple morphing applications*, Composite Structures, **207**, 598–611, 2019.
12. S. ÖZGEN, Y. YAMAN, M. ŞAHIN, G. SEBER, L. ÜNLÜSOY E. SAKARYA T. INSUYU, G. BAYRAM, Y. ULUDAD, A. YILMAZ, *Morphing air vehicle concepts*, International Unmanned Vehicle Workshop, Istanbul, Turkey, 2010.

13. C.L. Thill, J. Etches, I. Bond, K. Potter, P. Weaver, *Morphing skins*, The Aeronautical Journal, **112**, 117–139, 2008.

14. M.H. Fu, O.T. Xu, L.L. Hu, T.X. Yu, *Nonlinear shear modulus of re-entrant hexagonal honeycombs under large deformation*, International Journal of Solids and Structures, **80**, 284–296, 2016.

15. C. Qiu, Z. Guan, S. Jiang, Z. Li, *A method of determining effect elastic properties of honeycomb cores based on equal strain energy*, Chinese Journal of Aeronautics, **30**, 766–799, 2017.

16. R. Yazdanparast, R. Rafiee, *Developing a homogenization approach for estimation of in-plane effective elastic moduli of hexagonal honeycombs*, Engineering Analysis with Boundary Elements, **117**, 202–211, 2022.

17. K.R. Olympio, F. Gandhi, *Zero Poisson's ratio cellular honeycombs for flex skins undergoing one-dimensional morphing*, Journal of Intelligent Material Systems and Structures, **21**, 1737–1753, 2010.

18. X. Gong, J. Huang, F. Scarpa, Y. Liu, J. Leng, *Zero Poisson's ratio cellular structure for two-dimensional morphing applications*, Composite Structures, **134**, 384–392, 2015.

19. J. Huang, W. Liu, A. Tang, *Effects of fine-scale features on the elastic properties of zero Poisson's ratio honeycombs*, Materials Science and Engineering: B, **236**, 95–103, 2018.

20. W.D. Liu, H.D. Li, J. Zhang, *Elastic properties of a cellular structure with in-plane corrugated cosine beams*, Composite Structure, **180**, 251–262, 2017.

21. W.D. Liu, H.L. Li, J. Zhang, H.D. Li, *Elastic properties of a novel cellular structure with trapezoidal beams*, Aerospace Science and Technology, **75**, 315–328, 2018.

22. J. Chen, X. Shen, J. Li, *Zero Poisson's ratio flexible skin for potential two-dimensional wing morphing*, Aerospace Science and Technology, **45**, 228–241, 2015.

23. Y. Zhao, M. Ge, W. Ma, *The effective in-plane elastic of hexagonal honeycombs with consideration for geometric nonlinearity*, Composite Structures, **234**, 111749, 2020.

24. S. Malek, L. Gibson, *Effective elastic properties of periodic hexagonal honeycombs*, Mechanics of Materials, **91**, 226–240, 2015.

25. L. Song, Z. Yin, T. Wang, X. Shen, J. Wu, M. Su, *Nonlinear mechanics of a thin-walled honeycomb with zero Poisson's ratio*, Mechanics Based Design of Structures and Machines, **51**, 4977–4999, 2023.

26. L.H. Lan, M.H. Fu, *Nonlinear constitutive relations of cellular materials*, AIAA Journal, **47**, 264–270, 2009.

27. R. Zhong, M. Fu, Q. Yin, O. Xu, L. Hu, *Special characteristics of tetrachiral honeycombs under large deformation*, International Journal of Solids and Structures, **169**, 166–176, 2019.

28. G.A. Becus, *Homogenization and random evolutions: Applications to the mechanics of composite materials*, Journal of Applied Mathematics, **37**, 209–217, 1979.

29. J. Shigley, C. Mishke, R. Budynas, *Mechanical Engineering Design*, McGraw-Hill, New York, pp. 75–90, 2004.

30. S. Timoshenko, *Theory of Elastic Stability*, McGraw-Hill, New York, 1970.

31. J. SINGER, J. ARBOCAZ, T. WELLER, *Buckling Experiment Methods in Buckling of Thin-Walled Structures. Shell, Built-up Structures, Composites and Additional Topics*, John Wiley & Sons, New Jersey, 2002.

32. E.A. BUBERT, B.K.S. WOODS, K. LEE, C.S. KOTHERA, N.M. WERELEY, *Design and fabrication of a passive 1D morphing aircraft skin*, Journal of Intelligent Material Systems and Structures, **21**, 1699–1717, 2010.

33. M. DE SAINT-VENANT, *Memoire sur la Torsion des Prismes*, Memoir des Savants Etrangers, **14**, 233, 1855.

Received January 4, 2023; revised version September 20, 2023.
Published online October 31, 2023.